

MRS Communications (2020), 10, 230–241

© Materials Research Society, 2020

doi:10.1557/mrc.2020.30

Prospective Article

Strain Mediated Magneto-Electric Interactions in Hexagonal Ferrite and Ferroelectric Coaxial Nanofibers

Y. Liu,^{1,2} P. Zhou,^{1,2} J. Fu,^{1,3} M. Iyengar,¹ N. Liu,² P. Du,² Y. Xiong,⁴ V. Moiseienko,¹ W. Zhang,¹ J. Zhang,⁵ Z. Ma,² Y. Qi,² V. Novosad,⁴ T. Zhou,³ D. Filippov,⁶ T. Zhang,^{2 b)} M.E. Page,⁷ G. Srinivasan^{1 a)}

¹*Department of Physics, Oakland University, Rochester, MI 48309, USA*

²*Department of Materials Science and Engineering, Hubei University, Wuhan 430062, People's Republic of China*

³*College of Electronics and Information, Hangzhou Dianzi University, Hangzhou 310018, People's Republic of China*

⁴*Materials Science Division, Argonne National Laboratory, Argonne, IL 60439, USA*

⁵*College of Electrical and Information Engineering, Zhengzhou University of Light Industry, Zhengzhou 450002, People's Republic of China*

⁶*Novgorod State University, Veliky Novgorod, Russia*

⁷*Materials and Manufacturing Directorate, Air Force Research Laboratory, Wright-Patterson Air Force Base, Dayton, Ohio 45433, USA*

Abstract

This report is on the synthesis by electrospinning of multiferroic core-shell nanofibers of strontium hexaferrite and lead zirconate titanate or barium titanate and studies on magneto-electric (ME) coupling. Fibers with well-defined core-shell structures showed order parameters in agreement with values for nanostructures. The strength of ME coupling measured by magnetic field induced polarization showed fractional change in the remnant polarization as high as 21 %. The ME-voltage-coefficient in H-assembled films showed strong ME response for zero-magnetic bias field. Follow up studies and potential avenues for enhancing the strength of ME coupling in the core-shell nanofibers are discussed.

1. Introduction

Multiferroic composites of ferromagnetic and ferroelectric phases have been of interest for studies on the nature of coupling between the two ferroic phases and for use in sensor and high frequency device technologies.^[1-10] Such composites when subjected to a magnetic field H , for example, leads to deformation of the ferromagnetic phase due to magnetostriction. The strain when transferred to the ferroelectric phase will lead to an electrical response in the composite due to piezoelectric effects in the ferroelectric phase. The mechanical strain mediated response to a magnetic field is termed direct ME effect (DME) and its strength could be measured by ME voltage coefficient, magnetic field induced polarization, magneto-dielectric effect or magneto-capacitance effects.^[5-10] Response of the composites to an applied electric field E is termed converse ME effect (CME) and its strength can be measured by E -induced changes in the magnetization or anisotropy field. In recent years several groups reported on the observation of a giant DME effect in laminate, particulate and fibrous composites.^[7-16] Device applications for the composites include dual magnetic and electric field tunable microwave devices, sensors, and memory devices.^[17-21] An understanding of the ME coupling in the composites is therefore essential both for exploring avenues for enhancing its strength and for applications in useful technologies. Ferromagnetic and ferroelectric nanocomposites are of particular interest in this regard since they have a very high surface area-to-volume ratio that is a key ingredient for strong ME coupling.^[10, 22-24] Nanostructures studied so far include nanopillars, nanotubes, nanowires, and nanofibers.^[24-41] Core-shell nanowires are ideal structures to achieve strong ME coupling due to the absence of substrate clamping and loss of field induced strain due to clamping encountered in composites such as nanobilayer or nanopillars on a substrate.^[24-31]

This report is on ME effects in multiferroic nanofibers. Such fibers can be fabricated by electrospinning or blow spinning.^[24,42,43] Synthesis of coaxial fibers of spinel ferrites and ferroelectrics by electrospinning was reported by several groups.^[25-29] Several groups have synthesized ferrite-ferroelectric core-shell nanowires and tubes on porous anodized aluminum oxide or membrane templates by a combined sol-gel and electrochemical deposition techniques. Synthesis of fibers of ferrite-BTO with alternate or random

distribution of crystallites of the two phases was also reported. We prepared coaxial NFO-PZT or BTO nanowires by electrospinning.^[28,29] Wires 0.5-2 μm in diameter and 10-100 μm in length were obtained after annealing the fibers at 700 °C. Electron and scanning probe microscopy measurements showed the core-shell structure and ME interaction strengths were measured by polarization P versus electric field E under an applied H and magneto-dielectric effects. There were, however, very few studies on measurements of the strength of ME coupling in individual fibers that in general involved the use of piezo-response force (PFM)- or magnetic force (MFM) microscopy.^[38-41] In core-shell fibers of $\text{CoFe}_2\text{O}_4\text{-BiFeO}_3$ and $\text{CoFe}_2\text{O}_4\text{-Pb}(\text{Zr}_{0.52}\text{Ti}_{0.48})\text{O}_3$, PFM measurements were used to estimate the ME voltage coefficient (MEVC).^[38,39] The ME interaction strengths in nickel ferrite (NFO) and lead zirconate titanate (PZT) or barium titanate (BTO) core-shell fibers were measured by low frequency ME voltage coefficient and H induced ferroelectric polarization.^[28,29] Although models predict strong ME coupling, measured values of ME coupling were small compared to expected values.^[29]

A core-shell nanofiber system of importance is hexagonal ferrites and ferroelectrics since recent models predict very strong ME coupling these systems.^[22] The crystal structure of hexagonal ferrites is much more complex than spinel ferrites.^[43-45] They contain divalent Ba and/or Sr and trivalent Fe in both spinel (S) and hexagonal (R and T) blocks and are classified into M-, X-, Y-, Z-, W-, and U- types, depending on the nature and arrangements of spinel of hexagonal blocks. Antiferromagnetic alignment of Fe^{3+} in various crystallographic sites results in a net ferromagnetic moment. Hexagonal ferrites have very high magneto-crystalline anisotropy field, either uniaxial or planar, leading to a large remnant magnetization in these systems. In a composite of hexaferrite and ferroelectric, the remnant magnetization will act as a self-biasing field and the composite is expected to show strong DME under zero external bias.^[22] A very recent investigation on layered composites of PZT and polycrystalline platelets of W- or Y-type hexaferrites indeed reported the anticipated strong ME coupling in the absence of a bias magnetic field.^[31]

Here we discuss the synthesis by electrospinning and studies on the nature of ME effects in core-shell fibers of M-type hexaferrite and PZT or BTO. We choose ferrite with the composition $\text{SrFe}_{12}\text{O}_{19}$ (SrM) due

to higher magnetostriction and uniaxial anisotropy field compared to BaM.^[44,45] Since past studies on fibers of ferroelectric BTO^[45-50] and PZT with the composition $\text{PbZr}_{0.52}\text{Ti}_{0.48}\text{O}_3$ ^[51-56] reported order parameters in general agreement with values for thin films, we choose these ferroelectrics for composite fibers with SrM. For comparison, fibers of pure hexaferrite and ferroelectric phases were also synthesized and characterized in terms of ferroic order parameters. Fibers of SrM annealed at 800-1000 °C with average diameter of 220 nm had room temperature saturation magnetization of 72 emu/g in agreement with bulk value. Fibers of PZT and BTO annealed at high temperatures showed ferroelectric polarization smaller than polycrystalline thick films.^[50] Core-shell fibers of SrM/PZT and SrM/BTO imaged by a scanning microwave microscope (SMM) showed fibers of uniform diameter with the expected core and shell structure. The ferroic order parameters for the core-shell fibers were much smaller than the measured values for pure ferrite and ferroelectric fibers. Measurements on the strength of direct-ME interactions were done by static magnetic field induced polarization and low-frequency ME voltage coefficient in discs and 2D- and 3-D films of the discs assembled in a magnetic field. Assembly of millimeter or larger-scale nanomaterial superstructures can be achieved with H and /or E-fields. Traditional top-down lithographic techniques cannot be used for fabricating these structures, which are well-suited for useful applications. The measured ME strengths are comparable to reported values for spinel ferrite-PZT/BTO fiber composites, but were much smaller than theoretical estimates. We discuss possible paths for enhancing the ME interaction strengths in the hexaferrite-ferroelectric nanofiber composites.

2. Experimental Details

2.1 Synthesis of nanofibers by electrospinning

Electrospinning techniques were used for the synthesis of ferroic and multiferroic nanofibers and involved the following steps: (i) preparation of sol of ferrite and ferroelectrics, (ii) electrospinning by dispensing the sol in a syringe through a needle and by applying an electric field of 1 - 2 kV/cm between the needle and a rotating aluminium drum, and (iii) fibers are collected from the aluminium drum, dried at

50 °C for 24 hrs, and then annealed at high temperatures to form the ferroic phases.^[42,43,46-56] The fibers are formed from the sol droplets when the electrostatic force overcomes the force due to surface tension.

Strontium hexagonal ferrite $\text{SrFe}_{12}\text{O}_{19}$ (SrM) precursor solution was made with nitrates and 2,5-Dimethylfuran (DMF) at room temperature. Nitrates of Sr and Fe, 0.0441 g of $\text{Sr}(\text{NO}_3)_2$ and 1.01 g of $\text{Fe}(\text{NO}_3)_3 \cdot 9\text{H}_2\text{O}$, were dissolved in 7 ml of DMF solvent and stirred for 1 h. Then 0.56, 0.7 and 0.84 g of poly(vinylpyrrolidone) (PVP, $M_w \sim 1300000$) was added to the precursor solution and stirred for another 1 h to form the homogeneous sol with PVP concentration of 8 wt. %, 10 wt. %, and 12 wt. %.

The preparation for ferroelectric lead zirconate titanate $\text{PbZr}_{0.52}\text{Ti}_{0.48}\text{O}_3$ (PZT) and barium titanate BaTiO_3 (BTO) solutions are as follows. For PZT solution^[29], (i) 3.793 g of lead acetate trihydrate ($\text{Pb}(\text{CH}_3\text{CO}_2)_2 \cdot 3\text{H}_2\text{O}$, 99%) was added to 4 ml of 2-methoxyethanol then stirred and reflux for 1 h at 70 °C; (ii) 1.703 g of zirconium (IV) n-propoxide and 1.364 g of titanium (IV) isopropoxide were mixed with 0.2 g of acetic acid and 4 ml of 2-methoxyethanol; (iii) The two solutions were mixed together and refluxed for 3 h at 80 °C, then 0.5 ml of distilled water was added for hydrolysis and reflux for another 6 h at 80 °C; and (iv) PVP solution was made by dissolving 1.2 g of PVP to a mixture with 3 ml of ethanol and 9 ml of methanol, then the PVP solution was added to PZT precursor solution and stirred for 20 h at room temperature. As for BTO solution^[33], 1.275 g of barium acetate ($\text{Ba}(\text{CH}_3\text{COO})_2$, ACS, 99-102%) was dissolved in 4 ml of glacial acetic acid at room temperature. Then, 1.475 ml of titanium (IV) iso-propoxide $[(\text{CH}_3)_2\text{CHO}]_4\text{Ti}$, 97+%) was dropwise added with continuous stirring. Finally, the 3 ml of PVP solution (0.2 g PVP dissolved in 3 ml ethanol) were added and stirred at room temperature to form the mixture. The BTO solution was found to be very sensitive to the moisture and turns into gel since titanium iso-propoxide readily reacts with water.

For electrospinning the sol was loaded onto a syringe and placed in a syringe pump for ferrite or ferroelectric fibers and the sol was dispensed through an 18-gage stainless steel needle (rame-hart JG 18). Two separate syringes and a dual syringe pumping system were used for core-shell fibers and a coaxial stainless steel needle (rame-hart, JG 17-20) was used. The pumping rate of the sol was about 0.1 ml/h and the humidity inside the electrospinning chamber was kept at 35%. A DC voltage of 10 - 18 kV was applied

between the needle and a rotating aluminium drum at 10 cm away from the needle. As discussed later, the fiber diameter was found to be dependent on the viscosity of the sol and the strength of electric field applied during the fiber extraction. The as-spun fibers were collected on a rotating aluminium drum as well as on glass slides, dried in oven for 24 h at 50 °C and then annealed for 2 h at 700-1000 °C for ferroic fibers, and at 700-900 °C for SrM-PZT/BTO core-shell fibers.

2.2 Structural, ferroic and ME characterization of nanofibers

The structural characterization was carried out using a powder X-ray diffractometer (Bruker D8 advance, XRD) with Cu K α radiation, a scanning electron microscope (JEOL JSM 6510, SEM) and a scanning microwave microscope (Agilent Technology, SMM) composed of a standard (5420) atomic force microscopy (AFM) and a Vector Network Analyser (Agilent Technologies, PNAX). These systems were used for morphology, crystal structure and chemical composition by EDAX. Ferroelectric nature of the fibers was investigated by polarization P versus electric field E measurements with a Ferroelectric Tester (Radiant Technologies, Inc.). The magnetization for fibers was measured using a superconducting quantum interference device (SQUID).

The strength of ME interactions was measured by H-induced ferroelectric polarization in discs of the fibers and by measurements of the low-frequency ME voltage coefficient (MEVC) was on films of the fibers assembled in a magnetic field.^[28, 29] Data on P vs E under a static magnetic field H were obtained on discs of the fibers were pressed into a disc and annealed at 900 °C. Measurements of MEVC were done on both 2D- and 3D- films assembled in a magnetic field. The assembly of 2D-films was done between two electrodes on glass or Si substrates. 3D Films of thickness 70-100 μm were assembled between two Cu electrodes. A solution of fibers in ethyl alcohol mixed with a small amount of binder was placed on the substrates or Cu electrode, subjected to a uniform magnetic field (of an electromagnet) and left to dry. Data on MEVC were obtained by subjecting the film to a bias field H and an ac magnetic field H_{ac} at 30 Hz in the same direction as H. The ME voltage coefficient (MEVC) = $V/(t \times H_{ac})$ where V is the voltage measured

between electrodes and t is the electrode separation or film thickness and was measured as a function of H .^[10]

3. Results

3.1 Structural and magnetic properties of strontium hexagonal ferrite fibers

Figure 1(a) shows the SEM micrograph for as-spun SrM fibers under an electric field of 1.4 kV/cm with 12 wt. % of PVP. The randomly aligned fibers on a glass slide are of uniform diameter with an average diameter of 220 ~ 400 nm under different electric field. For SrM fibers with 8 wt. % of PVP with a much lower viscosity than for 12% PVP, a decrease in the average fiber diameter was measured. Annealing at temperatures 900 - 1000 °C led to a significant decrease in the fiber dimensions. Figure 1(b) is a profile of the number of fibers annealed at 900 °C as a function of diameter d measured with a SEM on 100 fibers. The results are for fibers obtained for a sol with 10 wt. % of PVP. A wide distribution in d ranging from 100 nm to 240 nm is evident, with 65% of the fibers with d in a narrow range 140 - 180 nm. Such fibers were used for measurements of ferroic order parameters and ME effects. The XRD pattern for SrM fibers annealed at 900 °C and 1000 °C are shown in Figure 1(c). The primary diffraction peaks are shown in the figure and except for the peaks corresponding to hexagonal SrM, there are no impurity phases present in the fibers. The magnetic properties for SrM fibers were investigated by measuring the magnetization M on annealed fibers. The room temperature M vs. H data for fibers annealed at 800 °C - 1000 °C are shown in Figure 1(d). Saturation of M occurs for $H \sim 20$ kOe with $M_s = 65$ -72 emu/g and the highest M_s is measured for fibers annealed at 1000 °C. The magnetization value agrees with $M_s = 76.7$ emu/g for bulk polycrystalline SrM.^[43]

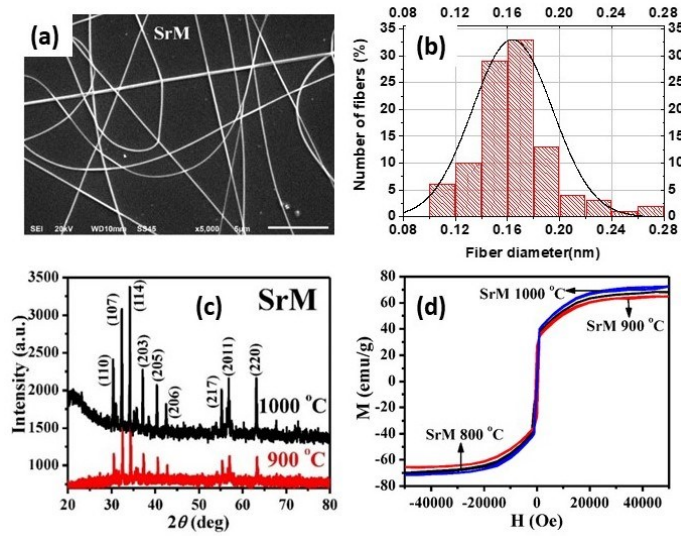


Figure 1. (a) SEM image for as-spun SrM fibers. (b) Number of fibers versus diameter profile for fibers annealed at 900 °C. (c) XRD data for SrM fibers annealed at 900 °C and 1000 °C. (d) Room temperature magnetization M vs. H for SrM fibers annealed at 800 °C, 900 °C, and 1000 °C.

3.2 Structural and ferroelectric characterization for PZT and BTO fibers

Both PZT and BTO fibers were synthesized by electrospinning under $E = 1$ kV/cm. The SEM image in Fig.2(a) for PZT shows fibers with uniform size and shape. Upon annealing at 900 °C the fibers had diameter in the range $d = 190$ nm - 650 nm. Figure 2(b) shows distribution in the diameter obtained from SEM image analysis for annealed fibers of BTO. Approximately 86% of the fibers have d -value of 500 - 700 nm. Figures 2(c) and (d) show the XRD data for PZT fibers annealed at 800 and 900 °C and BTO fibers annealed at 700 °C and 850 °C, respectively. The primary diffraction peaks were also shown in the figures. There is no impurity phase for BTO fibers, but there is a peak corresponding to TiO_2 (at 40°) for PZT fibers and some small peaks of PbO_2 for PZT annealed at 900 °C. The formation of TiO_2 may be due to reaction of titanium iso-propoxide in the sol with moisture.

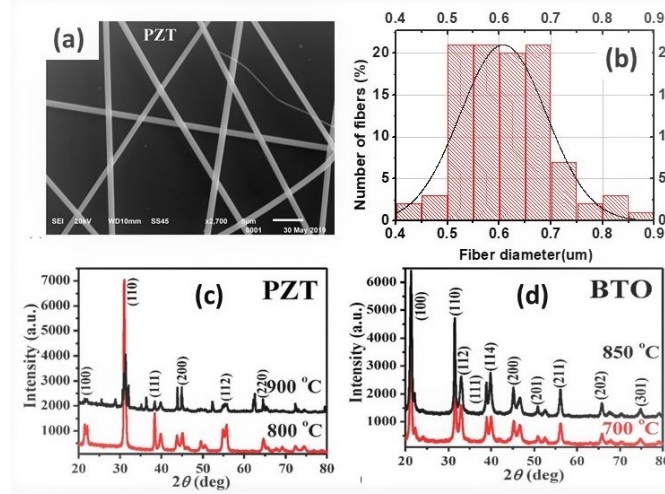


Figure 2. (a) SEM image for as-synthesized PZT fibers. (b) Number of fibers versus diameter for BTO fibers annealed at 900 °C. XRD data for (c) PZT fibers annealed at 800 °C and 900 °C and (d) BTO fibers annealed at 700 °C and 850 °C.

The ferroelectric nature for PZT and BTO fibers was investigated by measurements of polarization P vs electric field E and the results are shown in Figure 3. The polarization for PZT fiber has the highest remanent polarization $P_r = 0.64 \mu\text{C}/\text{cm}^2$ for measurements under $E = 27 \text{ kV}/\text{cm}$ which is much smaller than $12.2 \mu\text{C}/\text{cm}^2$ measured for $\text{Pb}(\text{Zr}_{0.6}\text{Ti}_{0.4})\text{O}_3$ fibers under $E = 55 \text{ kV}/\text{cm}$.^[53] The remanent polarization

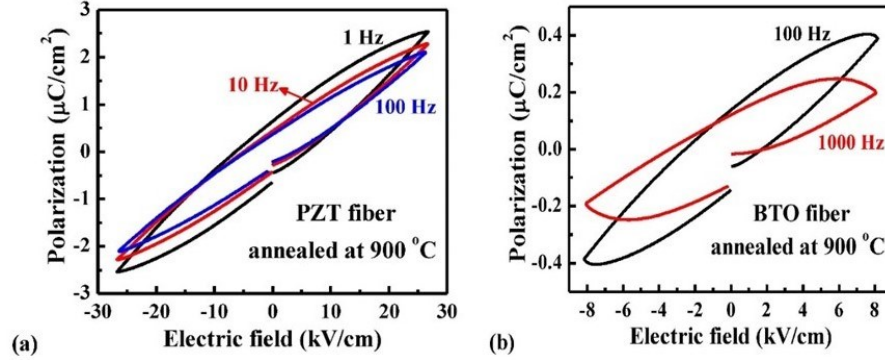


Figure 3. Polarization vs. E for disks of (a) PZT fibers and (b) BTO fiber annealed at 900 °C.

$P_r = 0.14 \mu\text{C}/\text{cm}^2$ at 100 Hz for BTO nanofiber compares favorably with the reported value for BTO fiber annealed at 1050 °C,^[47] but much smaller than for BTO microfiber which showed $P_r = 15.1 \mu\text{C}/\text{cm}^2$.^[48]

3.3 Multiferroic core-shell fibers

Two types of core-shell fibers, with ferroelectric core-SrM shell and SrM core-ferroelectric shell, were synthesized in our study. The fibers were spun under $E = 1.0 - 1.8 \text{ kV}/\text{cm}$, dried for 24 hrs at 50 °C,

and then annealed for 2 hrs at 700-900 °C. Both the heating and cooling rates were set at 0.25 to 0.5 °C/min in order to eliminate the possibility of blow holes and voids the the annealed fibers. Representative SEM image in Figure 4(a) for a fiber with $\sim 1 \mu\text{m}$ diameter SrM core and 500 nm thick BTO shell clearly shows the core and shell structure for the fiber annealed at 700 °C. Figure 4(b) shows the XRD data for fibers with either PZT or BTO core and SrM shell that were annealed at 900 °C. Both kind of fibers did not contain any impurity phases. The core-shell structure was further investigated by high frequency capacitance images obtained with a scanning microwave microscope (SMM). The SMM images for fibers with SrM core - BTO shell and SrM core - PZT shell are shown in Figures 5 (c)-(j), respectively. The images of topography, capacitance, and amplitude and phase of the scattering matrix S_{11} at 16-18 are shown. The core and shell structure is clearly seen in different contrasts for SrM and the ferroelectrics in all of the images.

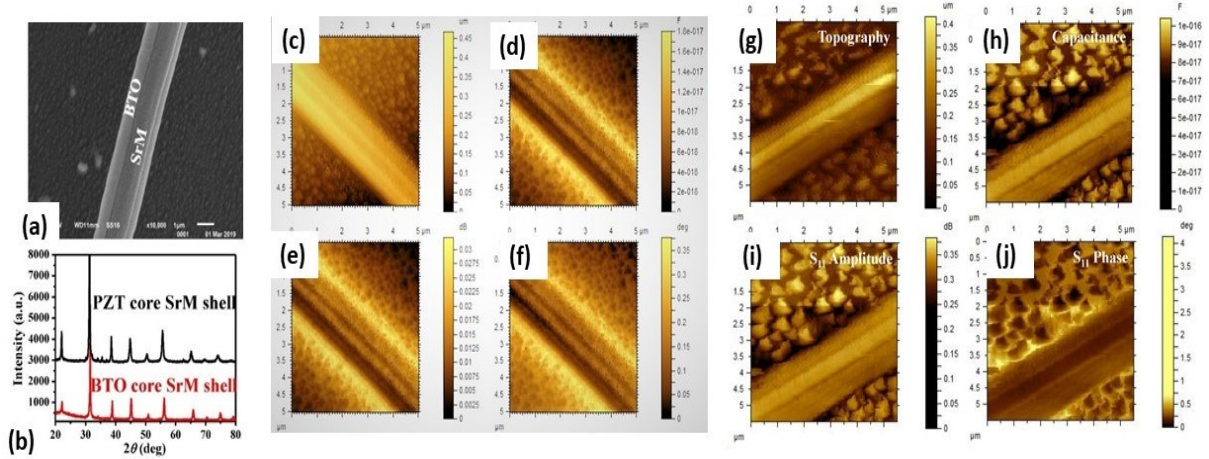


Figure 4. (a) SEM image for a fiber with SrM core-BTO shell annealed at 700 °C. (b) XRD data for PZT core-SrM shell and BTO core-SrM shell fibers annealed at 900 °C. Scanning microwave microscopy (SMM) images of topography [(c) and (g)], capacitance [(d) and (h)], S_{11} amplitude [(e) and (i)] and S_{11} phase [(f) and (j)] for annealed fibers of SrM core-BTO shell and SrM core-PZT shell, respectively.

The room temperature M vs. H for the core-shell fibers are shown in Figures 5(a) and (b). The data are for fibers with ferrite core (shell) and ferroelectrics shell (core) annealed at 900 °C. The measurements on BTO-SrM fibers show saturation of M for $H \sim 20$ kOe with $M_s \sim 2.5$ to 3.5 emu/g, whereas a slightly higher $M_s = 4 - 4.5$ emu/g is measured for SrM-PZT fibers. The relatively low M_s values are due to rather low volume (and weight) fraction of ferrite in the composites. From the dimensions of core and shell in the

SMM images in Fig.4, estimated volume fraction for SrM is 15% and the weight fraction is 11%. The M_s -values for fibers with SrM core corresponds to ferrite-only value of 32 emu/g for fibers with BTO shell and 47 emu/g for fibers with PZT core. These M_s -values are rather small compared to 72 emu/g for pure ferrite fibers in Figure 2 and the cause needs to be explored. The P vs. E data measured for disc of the fibers are shown in Figure 5(c) and (d). For fibers of PZT core - SrM shell, a remnant polarization $P_r = 1.42 \mu\text{C}/\text{cm}^2$ was measured for the loop obtained with $E = 43 \text{ kV}/\text{cm}$ at 1 Hz, which is smaller than $0.64 \mu\text{C}/\text{cm}^2$ for pure PZT fiber (Figure 3). The remnant polarization of $P_r = 0.035 \mu\text{C}/\text{cm}^2$ for SrM core - BTO shell is also much smaller than for pure BTO fiber. The P vs. E measurement was also carried out on SrM core - PZT shell and BTO core - SrM shell fiber disc, which show the remnant polarization of $0.19 \mu\text{C}/\text{cm}^2$ and $0.067 \mu\text{C}/\text{cm}^2$, respectively. Thus both M and P for the composite fibers are smaller than for ferrite and ferroelectric fibers.

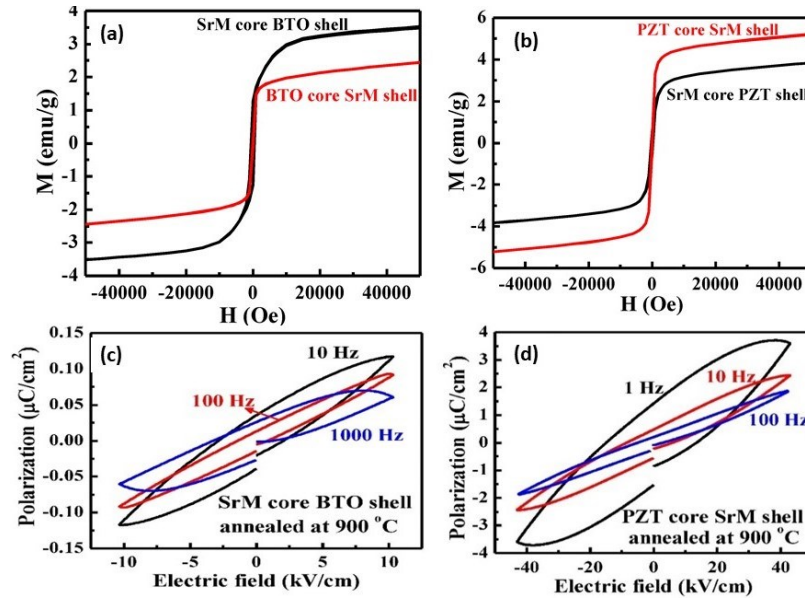


Figure 5. Room temperature magnetization M vs. H for (a) SrM-BTO and (b) SrM-BTO fibers annealed at 900 °C. Ferroelectric polarization P vs. E for (c) SrM-BTO and (d) SrM-PZT fibers at various frequencies.

The nature of ME effects for the core-shell fibers were studied by measuring the magnetic field induced polarization on a disk of the fibers. The disks were pressed with the fibers in a die and annealed at 900 °C. The P vs E under $H = 0$ to 6 kOe were done for all of the fibers and representative results are shown in Figure 6 for fibers of PZT core - SrM shell and SrM core - BTO shell. Estimated fractional change in P_r with H are shown in the figures. For both fibers $P_r(0)$ at $H = 0$ is higher than $P_r(H)$ under a magnetic field

H. The fractional change in P_r defined as $\Delta P_r/P_r = [P_r(H) - P_r(0)]/P_r(0)$, is also plotted as a function of H in Figure 6. The fractional change $\Delta P_r/P_r$ is negative and its magnitude is found to increase with increasing H. One also observes a hysteresis in the data. When H is decreased from 6 kOe to zero, the data in Figures 6(b) and (d) show a further decrease in the remnant polarization with decreasing H. For fibers with PZT core - SrM shell, $\Delta P_r/P_r$ decreased from 0 to -16.8% as H was increased from 0 to 6 kOe, then decreased to -21.3% when H was decreased back to 0 Oe. A similar behaviour is seen in Figure 6(d) for fibers of SrM core - BTO shell. Measurements done on fibers of SrM core - PZT shell and BTO core - SrM shell fibers also showed a decrease in P_r with increasing H and the magnitude of $\Delta P_r/P_r$ increased from 0 to 20% and 0 to 12%, respectively, as H was increased from 0 to 6 kOe.

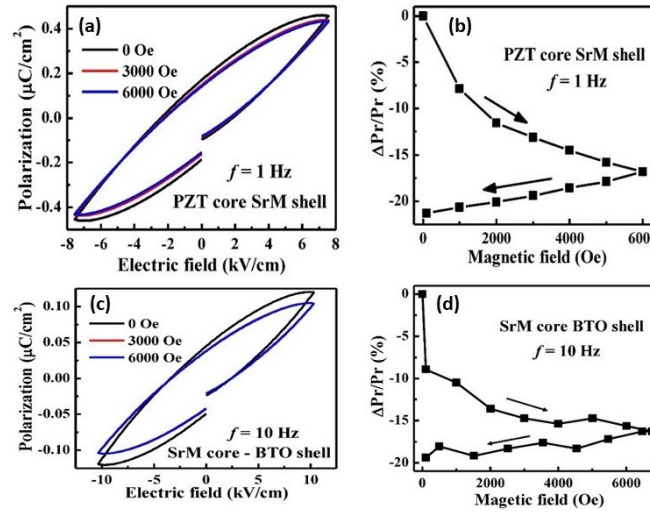


Figure 6. (a) Polarization P vs. E under H and (b) the estimated fractional change in P_r with H for a disc of fibers of (a) PZT core-SrM shell. (c) and (d) show similar data for a disc of fibers of SrM core-BTO shell.

The magneto-electric voltage coefficient (MEVC) measurements were carried out on two types of films assembled in a magnetic field: (i) fibers on a glass or Si substrate assembled into a 2D-film between two electrodes and (ii) 3D-film assembled between two electrodes. The H-assisted assembly was done with a uniform field produced by an electromagnet. The 2D-films were assembled on 5 mm × 5 mm substrates and between two 4 mm × 1 mm Ti-Pt electrodes separated by 2 mm. Fibers dispersed in a solvent were placed on the substrates and subjected to an in-plane field $H = 3$ kOe (directed perpendicular to the electrodes). For ME measurements, in-plane dc magnetic field H and an ac magnetic field $H_{ac} = 1$ Oe at 30

Hz were applied parallel to each other (and perpendicular to the electrodes). The ME voltage was measured between the electrodes and as a function of the bias field H . For measurements on 3D-films of thickness 70-100 μm assembled between two Cu electrodes, in-plane H and H_{ac} were applied parallel to each other and V was measured across the film thickness between the Cu electrodes.

The SEM image for a 2D-film of fibers of BTO core-SrM shell assembled on glass is shown in Figure 7(a). It is evident from the image that the fibers are aligned in the direction of applied field H . Figure 7(b) shows the MEVC vs H data for a film of SrM core-BTO shell. The data are for H and H_{ac} along the fiber alignment direction. The most significant observation in the data is the MEVC of 3.768 mV/cm·Oe for zero external bias field and could be attributed to a built-in bias field arising from magneto-crystalline anisotropy for the hexagonal ferrite. The MEVC has a maximum value of 3.852 mV/cm·Oe at $H = 7130$ Oe. Similar data in Figure 7(c) are for a film of fibers of SrM core - PZT shell on a glass slide. The zero-field MEVC is 3.14 mV/cm·Oe and the maximum value is 3.227 mV/cm·Oe at 7190 Oe.

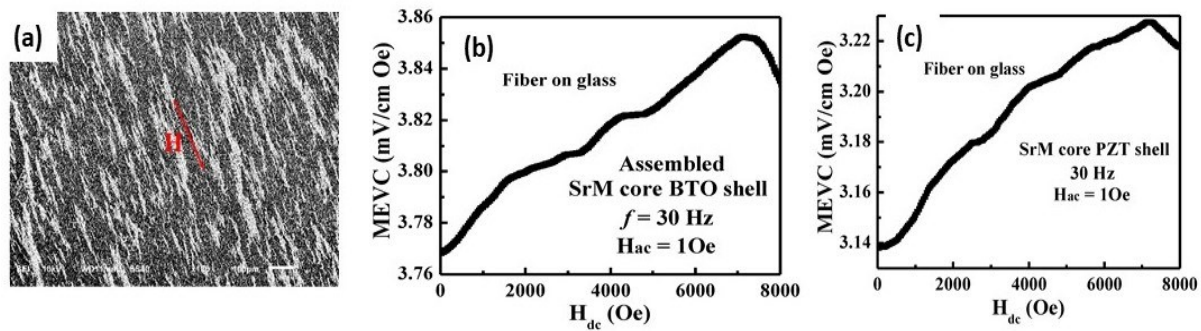


Figure 7. (a) SEM image for a planar film of H-assembled BTO core-SrM shell fibers on glass. The magneto-electric voltage coefficient MEVC vs. dc magnetic field at 30 Hz for H-assembled fiber films on glass for (b) SrM core-BTO shell and (c) SrM core-PZT shell.

The MEVC measurements were also done for 2D-films of BTO core - SrM shell and PZT core - SrM shell on glass which showed maximum MEVC values of 3.32 and 3.12 mV/cm·Oe, respectively.

Results of similar measurements of MEVC for 3D-films assembled between two electrodes in a magnetic field are shown in Figure 8. The data are for films of thickness 70-100 μm . A zero-bias ME coupling with a much higher MEVC than for 2D-films is seen in Figure 8. Fibers with SrM and BTO have a smaller ME voltage coefficient than for films with fibers of SrM and PZT. A key observation of

importance in Figure 8 is the higher MEVC for films with ferroelectric shell than for films with ferrite shell. Results in both Figures 7 and 8 show weak dependence of MEVC on H and could be attributed to a nearly constant value of the piezomagnetic coefficient $d\lambda/dH$, where λ is the magnetostriction for SrM, for the static field range H up to 8 kOe.

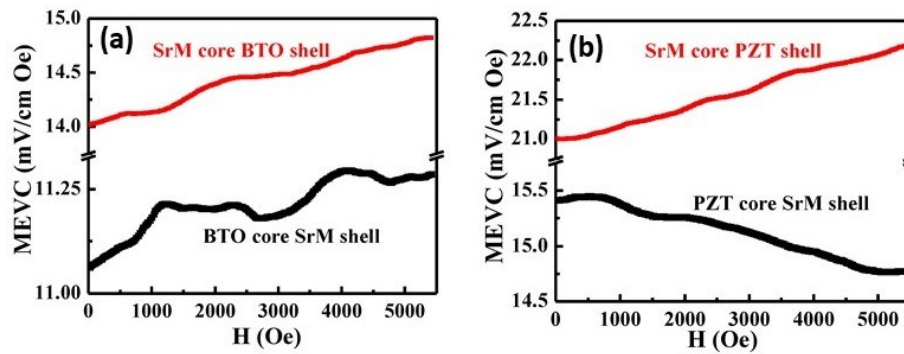


Figure 8. ME voltage coefficients versus H data as in Figure 7, but for 3D-films of core-shell fibers of (a) SrM-BTO and (b) SrM-PZT.

4. Discussion

Although the primary focus of this work was on multiferroic core-shell fibers, it was essential to study the nature of pure ferroic fibers for comparison of order parameters for both single phase and composite fibers. Results of this study clearly demonstrate the feasibility of synthesizing ferroic and multiferroic nanofibers by electrospinning. Fiber dimensions could be controlled with several parameters including the sol viscosity and the strength of the electric field applied between the needle and the collector. The profiles in Figures 1 and 2 for the distribution of fiber diameter indicate the potential for synthesizing 65% fibers with a deviation in diameter by $\pm 13\%$ and 85% of fibers with a deviation of $\pm 17\%$. In the case of ferroic fibers, X-ray diffraction data indicated the absence of impurity phases in annealed SrM and PZT fibers. For pure BTO fibers, however, it was necessary to anneal the fibers at or above 900 °C in order to eliminate the formation of non-ferroelectric cubic phase. We also inferred from our studies that heating and cooling rates for annealing the fibers will have to be on the order of 0.25 to 0.5 °C/min for obtaining fibers

free of voids and blow holes. Electron microscopy and scanning probe microscopy images for as-spun and annealed fibers revealed defect free and uniform ferroic fibers.

The ferroic order parameters for pure SrM, BTO and PZT fibers is considered next. Past studies on hexagonal ferrite fibers involved the use of blow spinning and annealing above 700 °C resulted in the formation of single phase SrM fibers with room temperature M_s of 81.2 emu/g. [57,58] Fibers of SrM prepared by electrospinning was reported to have a much smaller M_s of 64.5 emu/g. [59] In the present work eletrospun fibers of single phase SrM with $M_s \sim 72$ emu/g were obtained for annealing temperature T_a above 900 °C. For the ferroelectric fibers P vs E data in Figure 3 show a much smaller P_r compared to thin film values for BTO and PZT. [60,61] The ferroelectric order parameters for BTO fibers critically depend on the annealing temperature T_a . Previous studies on BTO fibers reported the formation of tetragonal perovskite phase for T_a above 700 °C. [46] In another recent study on BTO fibers, conversion of non-ferroelectric cubic phase to ferroelectric tetragonal was found occur for $T_a > 950$ °C and P vs E data for fibers for $T_a \sim 1050$ °C showed $P_r \sim 0.1$ $\mu\text{C}/\text{cm}^2$. [47] We also observed a significant amount of cubic phase in BTO fibers for $T_a = 700$ °C whereas annealing at 900 °C resulted in tetragonal phase with a small amount of hexagonal phase. The P vs E data in Figure 3(b) show $P_r \sim 0.1$ $\mu\text{C}/\text{cm}^2$ in agreement with the reported value in Ref.47. The reduction in P_r compared to thin films was attributed to grain boundaries in the nanocrystals in the fibers that give rise to clamping of domain walls and impede domain switching. [47] The data in Figure 3 shows a higher P_r of 0.5 $\mu\text{C}/\text{cm}^2$ for PZT fibers and is comparable to P_r of 1.5 $\mu\text{C}/\text{cm}^2$ measured for $E = 400$ kV/cm for PZT nanotube consisting of nanometer sized crystals. [62] Thus for both BTO and PZT fibers the saturation and remnant polarizations are at least an order of magnitude smaller compared to thin film or bulk values.

The core-shell structure for fibers of SrM and the ferroelectrics were confirmed by electron and scanning probe microscopy (Figure 4) and the annealed fibers were found to be free of impurity phases. We also inferred from SMM images that the SrM core diameter was small compared to the ferroelectric shell thickness. This is further confirmed by room temperature $M_s = 2.5 - 4.5$ emu/g for the annealed fibers in Figure 5. Assuming average size of fiber diameter and shell thickness in the SMM images of Figure 4,

one obtains a ferrite-only M_s of 32 emu/g which is a factor of 2 smaller than for pure ferrite fibers. The cause of this reduction in M_s for the core-shell fibers needs further investigation. A similar reduction in the magnetization was also reported for core shell fibers of nickel ferrite (NFO) and PZT and NFO-BTO. [28, 29] The remnant polarization values of 0.05 $\mu\text{C}/\text{cm}^2$ and 1 $\mu\text{C}/\text{cm}^2$ for the core-shell fibers of SrM with BTO and PZT, respectively, are comparable to values in Figure 3 for pure ferroelectric fibers.

The strength of ME coupling measured by H induced ferroelectric polarization on discs of the fibers are indicative of strong coupling in both SrM-BTO and SrM-PZT. The remnant polarization decreases in both systems with the application of H and the fractional change in P_r is higher in SrM-PZT than for SrM-BTO and could be due to higher polarization for fibers with PZT. Another observation of importance is the larger change in P_r measured for fibers with ferroelectric shell than for SrM shell and could be attributed to a higher leakage current expected for fibers with low resistivity ferrite than for fibers with ferroelectric shell. In our earlier studies on discs of randomly oriented fibers of NFO and PZT or BTO, we observed a fractional increase in P_r by 6% for $H = 7$ kOe whereas in the present system with hexagonal ferrites the change in P_r is a factor of 2 to 3 higher than in the spinel ferrite-ferroelectric fibers. [28,29] The H-induced polarization in bulk ferrite-ferroelectric composites and in single phase multiferroics show a much smaller change in P_r compared to the present system. [63,64]

The ME voltage coefficient data in Figure 7 for 2D-films assembled in a magnetic field is on the order of 3.1 to 3.9 mV/cm Oe with a large ME response for $H = 0$. Such zero-bias ME effects could be due to a self-biasing field arising from grading of ferroic order parameters or a remnant magnetization due to magnetocrystalline anisotropy. [65,66] The zero-bias MEVC in the data of Figure 7 is due to the uniaxial anisotropy field for M-type hexagonal ferrites that would give rise to a large remnant magnetization that acts as a built-in internal bias field. Another key observation in the data is the weak H dependence of MEVC for fields up to 8 kOe. The ME voltage coefficient is directly proportional to the piezomagnetic coefficient $q = d\lambda/dH$ where λ is the magnetostriction. Thus the MEVC vs H tracks the dependence of q on H and in the case of composites with spinel ferrites or soft magnetic materials MEVC drops to zero when λ attains

saturation and $q \sim 0$ at high bias fields. In the present case, however, it is clear that q remains almost constant for H up to 8 kOe. The ME voltage coefficients in Figure 7 is an order of magnitude higher than for H-assembled 2D films of NFO-PZT and NFO-BTO.^[28,29]

The MEVC data in Figure 8 for 3D films show a significant enhancement in the magnitude of MEVC compared to 2D films. The results are for in-plane parallel H and H_{ac} and ME voltage measured across the film thickness. A higher MEVC for samples with PZT than for films with BTO is likely due to superior ferroelectric order parameter for PZT that is evident in the P vs E data in Figure 5. Another observation, in agreement with the H -induced polarization, is the higher MEVC for samples with ferroelectric shell than for ferrite shell due to a smaller leakage current for the films with high resistivity ferroelectric shells. The ME response in Figures 7 and 8, however, is weak compared to measured MEVC values for layered composites of PZT and single crystal SrM.^[67] For the fiber films the strength of ME coupling is weakened due to several factors including electric and magnetic dipole-dipole interactions between fibers and film porosity. Although demagnetization effects will vanish for bias magnetic field and ac field along the fiber axis, the dipole-dipole coupling between magnetic cores or shells, fiber discontinuity in an assembled structure, porosity and voids in the films, in particular in the 2D films, will also contribute to weakening of sample magnetization and magnetostriction and lowering of ME voltages. Similarly, piezoelectric coefficient will be weakened due to electric dipole interaction between PZT or BTO cores or shells. Thus the ME voltage coefficient in 2D and 3D films will also be weaker compared to a free standing single nanofiber.

It is essential to carry out measurements of ME coupling in on single isolated fibers. Quantitative measurements of direct and converse-ME coupling could be done on stand-alone composite fibers placed on templates by nano-manipulation. Some of the suggested measurements in this regard include scanning probe microscopy techniques such as piezo-force microscopy under H , magnetic force microscopy under an applied voltage, ferromagnetic resonance under an electric field with an SMM, and MEVC measurements with nanoprobe.

Multiferroic core-shell fibers investigated here do show the potential to achieve strong ME coupling. Focused efforts that address the following are essential in order to realize coupling strengths predicted by theory.^[22] (i) Ferroic order parameters for cores and shells are measured to be much smaller than values for bulk materials and thin films. The fibers contain nanocrystallites and one has to understand the influence of their size and shape on the order parameters. (ii) Fibers with ferrite cores were found to have a much smaller diameter compared to ferroelectric shell thickness. Since the ME coupling is maximum for equal volume of the two ferroic phases, electrospinning synthesis parameters that control the core and shell dimensions need to be explored. (iii) Annealing temperatures for the fibers and heating and cooling rates are found to be key parameters that determine the crystallographic phases, size of nanocrystallites and pores and voids in the fibers. Undesired phases such as cubic BTO need to be eliminated for strong ME coupling. It is desirable to study the correlation between the fiber annealing parameters to ferroic order parameters. (iv) Fiber discs and 2D and 3D films used for ME measurements discussed in this study are susceptible to a large leakage current generally encountered in bulk composites and will lead to a significant reduction in the strength of ME coupling. Previously suggested ME measurements on isolated single fibers need to be performed for understanding the nature of ME interactions in the composites. (v) Finally, the study has to be expanded to include Y- and W-type hexaferrites since one may realize a much higher magnetostriction and ME coupling strength than for composites with M-type ferrites. Composites with fibers of Y-type ferrites ($\text{Ba}_2\text{Me}_2\text{Fe}_{12}\text{O}_{22}$, Me = Ni, Zn) that have uniaxial anisotropy; or W-type ferrites $\text{Ba Me}_2 \text{Fe}_{16} \text{O}_{27}$ (Me = Co, Zn) with uniaxial or planar anisotropy are potential candidate materials for follow up studies.

There has been considerable interest in recent years in composite multiferroics. This report therefore addresses a new family of multiferroic nanomaterials with potential for achieving strong ME coupling. It is necessary to explore the paths for synthesizing nanofibers with order parameters comparable to bulk materials. It is also necessary to come up with a viable path for instantaneous assembly of the nanofibers into superstructures. Measurements of ME coupling in nano-fibers and comparison measurements on assemblies will lead to a basic understanding of the nature of electromagnetic interactions and applications in sensor and signal processing technologies. In addition, local measurement for the individual fibers may help unambiguously reveal the physical origin of these various coupling effects. We anticipate new

phenomena, theory, and novel applications to emerge from this research. We summarize the details of the 3-year program in Table 2 below.

5. Conclusions

Nanofibers of M-type Sr-hexaferrite and ferroelectric PZT and BTO and coaxial ferrite-ferroelectric fibers have been synthesized by electrospinning. Pure ferrite and ferroelectric fibers were of uniform diameter that could be controlled with sol viscosity and electric field applied during electrospinning. Electron and scanning probe microscopy images revealed fibers of uniform diameter. Annealed fibers were characterized in terms of order parameters. The saturation magnetization for SrM fiber agreed with the values expected for bulk ferrites. The polarization values for PZT and BTO fibers agreed with past reports for fibers, but were smaller than the bulk values. Images obtained by scanning microwave microscopy showed core-shell structures for the composite nanowires with the diameter in the range 220 ~ 1000 nm. The multiferroic coaxial fibers, however, showed a smaller saturation magnetization or remnant polarization compared to values for pure ferroic fibers. The strength of magnetoelectric interactions were measured by magnetic field induced polarization and ME voltage coefficient. The remnant polarization decreased with the application of H in all of the fiber samples, with a decrease as high as 20% for SrM-PZT fibers. The MEVC was measured for both 3D and 2D fiber films assembled in a magnetic field. Both types of films had a large zero-bias ME response and the 3D films showed a higher MEVC of 14 - 22 mV/cm·Oe than 3.2 – 3.8 mV/cm·Oe for 2D films. The ME interaction strengths for coaxial fibers studied here are smaller than predicted by theory. Follow up studies on control of fibers parameters aimed at improving the ferroic order parameters are essential. Efforts also must focus on obtaining fibers with equal volume fraction of ferromagnetic and ferroelectric phase to enhance the ME coupling strengths. It is also necessary to study the correlation between fiber diameter, size of nano-crystallites in the fibers, ferroic order parameters and ME coupling. Finally, the nature of magneto-electric effects in single fiber must be

performed for better understanding of the ME coupling in these nanostructures and to explore potential applications in sensors and advanced technologies.

Acknowledgements

The research at Oakland University was supported by grants from the National Science Foundation (DMR-1808892, ECCS-1923732). Ying Liu was supported by a fellowship from the Chinese Scholarship Council. The research at AFRL was partially supported by the Air Force Office of Scientific Research (AFOSR) Award No. FA9550-20RXCOR074, and a Summer Faculty Fellowship for G.S. Efforts at the Argonne National Laboratory were supported by a grant from the DOE-BSE-Materials Science and Engineering Division.

Caption for Figures

Figure 1. (a) SEM image for as-spun SrM fibers. (b) Number of fibers versus diameter profile for fibers annealed at 900 °C. (c) XRD data for SrM fibers annealed at 900 °C and 1000°C. (d) Room temperature magnetization M vs. H for SrM fibers annealed at 800 °C, 900 °C, and 1000 °C.

Figure 2. (a) SEM image for as-synthesized PZT fibers. (b) Number of fibers versus diameter for BTO fibers annealed at 900 °C. XRD data for (c) PZT fibers annealed at 800 °C and 900 °C and (d) BTO fibers annealed at 700 °C and 850 °C.

Figure 3. Polarization vs. E for disks of (a) PZT fibers and (b) BTO fiber annealed at 900 °C.

Figure 4. (a) SEM image for a fiber with SrM core-BTO shell annealed at 700 °C. (b) XRD data for PZT core-SrM shell and BTO core-SrM shell fibers annealed at 900 °C. Scanning microwave microscopy (SMM) images of topography [(c) and (g)], capacitance [(d) and (h)], S_{11} amplitude [(e) and (i)] and S_{11} phase [(f) and (j)] for annealed fibers of SrM core-BTO shell and SrM core-PZT shell, respectively.

Figure 5. Room temperature magnetization M vs. H for (a) SrM -BTO and (b) SrM-BTO fibers annealed at 900 °C. Ferroelectric polarization P vs. E for (c) SrM-BTO and (d) SrM-PZT fibers at various frequencies.

Figure 6. (a) Polarization P vs. E under H and (b) the estimated fractional change in P_r with H for a disc of fibers of (a) PZT core-SrM shell. (c) and (d) show similar data for a disc of fibers of SrM core-BTO shell.

Figure 7. (a) SEM image for a planar film of H-assembled BTO core-SrM shell fibers on glass. The magneto-electric voltage coefficient MEVC vs. dc magnetic field at 30 Hz for H-assembled fiber films on glass for (b) SrM core-BTO shell and (c) SrM core-PZT shell.

Figure 8. ME voltage coefficients versus H data as in Figure 7, but for 3D-films of core-shell fibers of (a) SrM-BTO and (b) SrM-PZT.

References

1. C. Nan: Magnetoelectric effect in composites of piezoelectric and piezomagnetic phases. *Phys. Rev. B* **50**, 9 (1994).
2. J. Ryu, S. Priya, K. Uchino, and H.E. Kim: Magnetoelectric effect in composites of magnetostrictive and piezoelectric materials. *J. Elec.* **8**, 2 (2002).
3. W. Eerenstein, N.D. Mathur, and J.F. Scott: Multiferroic and magnetoelectric materials. *Nature* **442**, 7104 (2006).
4. R. Ramesh and N.A. Spaldin: Multiferroics: progress and prospects in thin films. *Nat. Mater.* **6**, 21 (2007).
5. C. Nan, M.I. Bichurin, S. Dong, D. Viehland, and G. Srinivasan: Multiferroic magnetoelectric composites: Historical perspective, status, and future directions. *J. Appl. Phys.* **103**, 3 (2008).
6. J. Zhai, Z. Xing, S. Dong, J. Li, and D. Viehland: Magnetoelectric laminate composites: an overview. *J. Am. Ceram. Soc.* **91**, 2 (2008).
7. S. Priya, R. Islam, S. Dong, and D. Viehland: Recent advancements in magnetoelectric particulate and laminate composites. *J. Elec.* **19**, 1 (2007).
8. G. Srinivasan: Magnetoelectric composites. *Annu. Rev. Mater. Res.* **40**, 153-178 (2010).
9. J. Cui, J.L. Hockel, P K. Nordeen, D.M. Pisani, C. Liang, G.P. Carman, and C.S. Lynch: A method to control magnetism in individual strain-mediated magnetoelectric islands. *Appl. Phys. Lett.* **103**, 23 (2013).
10. G. Srinivasan, S. Priya, and N.X. Sun: Composite magnetoelectrics: materials, structures, and applications. *Elsevier* (2015).
11. V. Corral-Flores, D. Bueno-Baques, D. Carrillo-Flores, and J.A. Matutes-Aquino: Enhanced magnetoelectric effect in core-shell particulate composites. *J. Appl. Phys.* **99**, 8 (2006).
12. R.S. Devan, and B.K. Chougule: Effect of composition on coupled electric, magnetic, and dielectric properties of two phase particulate magnetoelectric composite. *J. Appl. Phys.* **101**, 1 (2007).
13. H. Yang, G. Zhang, Y. Lin, T. Ye, and P. Kang: Electrical, magnetic and magnetoelectric properties of BaTiO₃/BiY₂Fe₅O₁₂ particulate composites. *Ceram. Int.* **41**, 5 (2015).
14. Y. Benveniste: Magnetoelectric effect in fibrous composites with piezoelectric and piezomagnetic phases. *Phys. Rev. B* **51**, 22 (1995).
15. L.P. Liu, and H.Y. Kuo: Closed-form solutions to the effective properties of fibrous magnetoelectric composites and their applications. *Int. J. Solids Struct.* **49**, 22 (2012).
16. H.Y. Kuo, and Y.L. Wang: Optimization of magnetoelectricity in multiferroic fibrous composites. *Mech. Mater.* **50**, 88-99 (2012).

17. J. Hu, Z. Li, J. Wang, and C.W. Nan: Electric-field control of strain-mediated magnetoelectric random access memory. *J. Appl. Phys.* **107**, 9 (2010).
18. N.X. Sun, and G. Srinivasan: Voltage control of magnetism in multiferroic heterostructures and devices. *Spin, World Scientific Publishing Company* **2**, 1240004 (2012).
19. M.M. Vopson: Fundamentals of multiferroic materials and their possible applications. *Crit. Rev. Solid State Mater. Sci.* **40**, 223-250 (2015).
20. C.M. Leung, J.F. Li, D. Viehland, and X. Zhuang: A review on applications of magnetoelectric composites: from heterostructural uncooled magnetic sensors, energy harvesters to highly efficient power converters. *J. Phys. D: Appl. Phys.* **51**, 263002 (2018).
21. D. Viehland, M. Wuttig, J. McCord, and E. Quandt: Magnetoelectric magnetic field sensors. *MRS Bull.* **43**, 834-840 (2018).
22. V.M. Petrov, J. Zhang, H. Qu, P. Zhou, T. Zhang, and G. Srinivasan: Theory of magnetoelectric effects in multiferroic core-shell nanofibers of hexagonal ferrites and ferroelectrics. *J. Phys. D: Appl. Phys.* **51**, 28 (2018).
23. C. Vaz, J. Hoffman, C.H. Ahn, and R. Ramesh: Magnetoelectric coupling effects in multiferroic complex oxide composite structures. *Adv. Mater.* **22**, 2900-2918 (2010).
24. D. Viehland, J.F. Li, Y. Yang, T. Costanzo, A. Yourdkhani, G. Caruntu, P. Zhou, T. Zhang, T. Li, A. Gupta, M. Popov, and G. Srinivasan: Tutorial: Product properties in multiferroic nanocomposites. *J. Appl. Phys.* **124**, 061101 (2018).
25. X.Z. Chen, M. Hoop, N. Shamsudhin, T. Huang, B. Özkale, Q. Li, E. Siringil, F. Mushtaq, L. Di Tizio, B.J. Nelson, and S. Pané: Hybrid magnetoelectric nanowires for nanorobotic applications: fabrication, magnetoelectric coupling, and magnetically assisted in vitro targeted drug delivery. *Adv. Mater.* **29**, 8 (2017).
26. S. Xie, F. Ma, Y. Liu, and J. Li: Multiferroic $\text{CoFe}_2\text{O}_4\text{-Pb}(\text{Zr}_{0.52}\text{Ti}_{0.48})\text{O}_3$ core-shell nanofibers and their magnetoelectric coupling. *Nanoscale* **3**, 8 (2011).
27. Q. Zhu, Y. Xie, J. Zhang, Y. Liu, Q. Zhan, H. Miao, and S. Xie: Multiferroic $\text{CoFe}_2\text{O}_4\text{-BiFeO}_3$ core-shell nanofibers and their nanoscale magnetoelectric coupling. *J. Mater. Res.* **29**, 5 (2014).
28. G. Sreenivasulu, M. Popov, R. Zhang, K. Sharma, C. Janes, A. Mukundan, and G. Srinivasan: Magnetic field assisted self-assembly of ferrite-ferroelectric core-shell nanofibers and studies on magneto-electric interactions. *Appl. Phys. Lett.* **104**, 5 (2014).
29. G. Sreenivasulu, J. Zhang, R. Zhang, M. Popov, V. Petrov, and G. Srinivasan: Multiferroic core-shell nanofibers, assembly in a magnetic field, and studies on magneto-electric interactions. *Materials* **11**, 1 (2018).

30. G. Caruntu, A. Yourdkhani, M. Vopsaroiu, and G. Srinivasan: Probing the local strain-mediated magnetoelectric coupling in multiferroic nanocomposites by magnetic field-assisted piezoresponse force microscopy. *Nanoscale* **4**, 3218-3227 (2012).
31. Y. Liu, J. Zhang, P. Zhou, C. Dong, X. Liang, W. Zhang, T. Zhang, N.X. Sun, D. Filippov, and G. Srinivasan: Magneto-electric interactions in composites of self-biased Y-and W-type hexagonal ferrites and lead zirconate titanate: Experiment and theory. *J. Appl. Phys.* **126**, 114102 (2019).
32. J.H. Li, I. Levin, J. Slutsker, V. Provenzano, P. K. Schenck, R. Ramesh, J. Ouyang, and A.L. Roytburd: Self-assembled multiferroic nanostructures in the $\text{CoFe}_2\text{O}_4\text{-PbTiO}_3$ system. *Appl. Phys. Lett.* **87**, 072909 (2005).
33. H. Zheng, J. Wang, S.E. Lofland, Z. Ma, L. Mohaddes-Ardabili, T. Zhao, L. Salamanca-Riba, S.R. Shinde, S.B. Ogale, F. Bai, D. Viehland, Y. Jia, D.G. Schlom, M. Wuttig, A. Roytburd, and R. Ramesh: Multiferroic $\text{BaTiO}_3\text{-CoFe}_2\text{O}_4$ nanostructures. *Science* **303**, 661-663 (2004).
34. X.S. Gao, B.J. Rodriguez, L. Liu, B. Birajdar, D. Pantel, M. Ziese, M. Alexe, and D. Hesse: Microstructure and properties of well-ordered multiferroic $\text{Pb}(\text{Zr,Ti})\text{O}_3/\text{CoFe}_2\text{O}_4$ nanocomposites. *ACS Nano* **4**, 1099 (2010).
35. I. Vrejoiu, A. Morelli, D. Biggemann, and E. Pippel: Ordered arrays of multiferroic epitaxial nanostructures. *Nano Rev.* **2**, 7364 (2011).
36. Y. Yang, S. Priya, J. Li, and D. Viehland: Two-phase coexistence in single-grain $\text{BaTiO}_3\text{-(Mn}_{0.5}\text{Zn}_{0.5})\text{Fe}_2\text{O}_4$ composites, via solid-state reaction. *J. Am. Ceram. Soc.* **92**, 1552 (2009).
37. F. Bai, H. Zhang, J. Li, and D. Viehland: Magnetic and magnetoelectric properties of as-deposited and annealed $\text{BaTiO}_3\text{-CoFe}_2\text{O}_4$ nanocomposite thin films. *J. Phys.D: Appl. Phys.* **43**, 285002 (2010).
38. L. Li, Lu Lu, Dawei Zhang, Ran Su, Guang Yang, Junyi Zhai, and Yaodong Yang: Direct Observation of Magnetic Field Induced Ferroelectric Domain Evolution in Self-Assembled Quasi (0-3) $\text{BiFeO}_3\text{-CoFe}_2\text{O}_4$ Thin Films. *ACS Appl. Mater. Interfaces* **8**, 442 (2015).
39. G. Caruntu, A. Ypurdkhani, M. Vopsaroiu, and G. Srinivasan: Probing the local strain-mediated magnetoelectric coupling in Multiferroic nanocomposites by magnetic field-assisted piezoresponse microscopy. *Nanoscale* **4**, 3218 (2012).
40. Z.H. Hua, P. Yang, H.B. Huang, J.G. Wan, Z.Z. Yu, S.G. Yang, M. Lu, B.X. Gu, and Y.W. Du: Sol-gel template synthesis and characterization of magnetoelectric $\text{CoFe}_2\text{O}_4/\text{Pb}(\text{Zr}_{0.52}\text{Ti}_{0.48})\text{O}_3$ nanotubes. *Mater.Chem. Phys.* **107**, 541-546 (2008).
41. M. Liu, X. Li, H. Imrane, Y.J. Chen, T. Goodrich, Z.H. Cai, K.S. Ziemer, J.Y. Huang, and N.X. Sun: Synthesis of ordered arrays of multiferroic $\text{NiFe}_2\text{O}_4\text{-Pb}(\text{Zr}_{0.52}\text{Ti}_{0.48})\text{O}_3$ core-shell nanowires. *Appl. Phys. Lett.* **90**, 152501 (2007).
42. R.C. Pullar: Hexagonal ferrite fibres and nanofibres. *Solid State Phenom.* **241**, 1-68 (2016).

43. R.C. Pullar: Hexagonal ferrites: a review of the synthesis, properties and applications of hexaferrite ceramics. *Prog. Mater. Sci.* **57**, 1191-1334 (2012).
44. R.C. Pullar, M.D. Taylor, and A.K. Bhattacharya: A halide free route to the manufacture of microstructurally improved M ferrite ($\text{BaFe}_{12}\text{O}_{19}$ and $\text{SrFe}_{12}\text{O}_{19}$) fibres. *J. Eur. Ceram. Soc.* **22**, 12 (2002).
45. R. Sun, X. Li, A. Xia, S. Su, and C. Jin: Hexagonal $\text{SrFe}_{12}\text{O}_{19}$ ferrite with high saturation magnetization. *Ceram. Int.* **44**, 12 (2018).
46. J. Yuh, J.C. Nino, and W.M. Sigmund: Synthesis of barium titanate (BaTiO_3) nanofibers via electrospinning. *Mater. Lett.* **59**, 28 (2005).
47. Y. Wei, Y. Song, X. Deng, B. Han, X. Zhang, Y. Shen, and Y. Lin: Dielectric and ferroelectric properties of BaTiO_3 nanofibers prepared via electrospinning. *J. Mater. Sci. Tech.* **30**, 8 (2014).
48. Z. Miao, L. Chen, F. Zhou, and Q. Wang: Modulation of resistive switching characteristics for individual BaTiO_3 microfiber by surface oxygen vacancies. *J. Phys. D: Appl. Phys.* **51**, 2 (2017).
49. H. Tang, Z. Zhou, and H.A. Sodano: Relationship between BaTiO_3 nanowire aspect ratio and the dielectric permittivity of nanocomposites. *ACS Appl. Mater. Interfaces* **6**, 5450-5455 (2014).
50. K.J. Choi, M. Biegalski, Y.L. Li, A. Sharan, J. Schubert, R. Uecker, P. Reiche Y.B. Chen, X.Q. Pan, V. Gopalan, L.Q. Chen, D.G. Schlom, C.B. Eom: Enhancement of ferroelectricity in strained BaTiO_3 thin films. *Science* **306**, 1005-1009 (2004).
51. Zhao Wang, Xumin Pan, Yahua He, Yongming Hu, Haoshuang Gu, and Yu Wang: Piezoelectric nanowires in energy harvesting applications. *Adv. Mater. Sci. Eng.* **2015**, 165631 (2015).
52. X. Chen, S. Xu, N. Yao, W. Xu, and Y. Shi: Potential measurement from a single lead zirconate titanate nanofiber using a nanomanipulator. *Appl. Phys. Lett.* **94**, 253113 (2009).
53. K.H. Cho, and S. Priya: Synthesis of ferroelectric PZT fibers using sol-gel technique. *Mater. Lett.* **65**, 4 (2011).
54. H.N. Lee, S.M. Nakhmanson, M.F. Chisholm, H.M. Christen, K.M. Rabe, and D. Vanderbilt: Suppressed dependence of polarization on epitaxial strain in highly polar ferroelectrics. *Phys. Rev. Lett.* **98**, 21 (2007).
55. M. Fan, W. Hui, Z. Li, Z. Shen, H. Li, A. Jiang, and Y. Chen: Fabrication and piezoresponse of electrospun ultra-fine $\text{Pb}(\text{Zr}_{0.3}\text{Ti}_{0.7})\text{O}_3$ nanofibers. *Microelectronic Eng.* **98**, 371 (1998).
56. M. H. Malakooti, Zhi Zhou, and Henry A. Sodano: Enhanced energy harvesting through nanowire based functionally graded interfaces. *Nano Energy* **52**, 171-182 (2018).
57. R.C. Pullar, M.D. Taylor, and A.K. Bhattacharya: Halide removal from BaM ($\text{BaFe}_{12}\text{O}_{19}$) and SrM ($\text{SrFe}_{12}\text{O}_{19}$) ferrite fibers via a steaming process. *J. Mater. Res.* **16**, 3162-3169 (2001).

58. R.C. Pullar, I.K. Bdikin, and A.K. Bhattacharya: Magnetic properties of randomly oriented BaM, SrM, Co₂Y, Co₂Z and Co₂W hexagonal ferrite fibres. *J. Eur. Ceram. Soc.* **32**, 905-913 (2012).
59. M.Q. Liu, X.Q. Shen, X.F. Meng, F.Z. Song, and J. Xiang: Fabrication and magnetic property of M-type strontium ferrite nanofibers by electrospinning. *J. Inorg. Mater.* **1** (2010).
60. P. Muralt, M. Kohli, T. Maeder, A. Kholkin, K. Brooks, N. Setter, and R. Luthier: Fabrication and characterization of PZT thin-film vibrators for micromotors. *Sens. Actuators A: Phys.* **48**, 157-165 (1995).
61. K. Kajiyoshi, N. Ishizawa, and M. Yoshimura: Preparation of tetragonal barium titanate thin film on titanium metal substrate by hydrothermal method. *J. Am. Ceram. Soc.* **74**, 369-374 (1991).
62. J. Kim, S.A. Yang, Y.C. Choi, J.K. Han, K.O. Jeong, Y.J. Yun, D.J. Kim, S.M. Yang, D. Yoon, H. Cheong, K.S. Chang, T.W. Noh, S.D. Bu: Ferroelectricity in highly ordered arrays of ultra-thin-walled Pb(Zr,Ti)O₃ nanotubes composed of nanometer-sized perovskite crystallites. *Nano lett.* **8**, 1813-1818 (2008).
63. S. Liu, S. Yan, H. Luo, S. Huang, C. Liao, and L. Deng: Magnetic effects on polarization response in particulate magnetoelectric Bi_{0.5}Na_{0.5}TiO₃-La_{0.67}Sr_{0.33}MnO₃ composites. *Mater. Lett.* **212**, 139 (2018).
64. G. Lawes and G. Srinivasan: Introduction to magnetoelectric coupling and multiferroic films. *J. Phys. D: Appl. Phys.* **44**, 243001 (2011).
65. S.C. Yang, C.S. Park, K.H. Cho, and S. Priya: Self-biased magnetoelectric response in three-phase laminates. *J. Appl. Phys.* **108**, 093706 (2010).
66. Y. Zhou, D. Maurya, Y. Yan, G. Srinivasan, E. Quandt, and S. Priya: Self-biased magnetoelectric composites: An overview and future perspectives. *Energy Harvesting Syst.* **3**, 42 (2016).
67. V. L. Mathe, G. Srinivasan, and A. M. Balbashov: Magnetoelectric effects in bilayers of lead zirconate titanate and single crystal hexaferrites. *Appl. Phys. Lett.* **92**, 122505 (2008).